3D crustal velocity and V_P/V_S structures beneath Southeast Anatolia and their geodynamic implications

M. K. Salah[1], Ş. Şahin[2], 2019

[1]Department of Geology, American University of Beirut, Beirut, Lebanon
[2]Department of Geophysics, Suleyman Demirel University, Isparta, Turkey
Received 14 November 2018

Застосовано метод сейсмічної томографії до даних щодо часу вступу поздовжніх і поперечних хвиль від локальних корових землетрусів у Південно-Східній Анатолії для вивчення дрібних тривимірних швидкісних структур і співвідношення V_P/V_S під цим регіоном. Багато попередніх сейсмологічних досліджень регіону виконано на регіональному або навіть глобальному рівні. У цілому з 2150 ретельно відібраних подій, що генерують 13690 і 12560 часів вступу P- і S-хвиль, було використано в томографічній інверсії. За результатами тестування на розв'язання «шахової» задачі припускають, що отримані аномалії швидкості та співвідношення V_P/V_S відображають особливості будови розрізу. Великі поперечні неоднорідності кори у вигляді аномалій швидкості нижче середньої виявлено під Південно-Східною Анатолією. Слабкі аномалії швидкості відображаються поблизу сегментів з активними порушеннями. Крім того, високі співвідношення V_P/V_S закартовано поблизу основних поділів земної кори, особливо на глибинах 10 і 22 км, що узгоджується з розміщенням офіолітових поясів. Зони високих співвідношень V_P/V_S викликані можливим існуванням у корі та, можливо, у верхній частині мантії флюїдів, що зазнають до надвисокого тиску. Поява цих флюїдів за інтенсивної тектонічної активності може стати пусковим механізмом для великих корових землетрусів уздовж західного сегмента Східноанатолійської зони порушень. Це землетруси можливі в зонах високих швидкостей, однак більшість великих корових землетрусів розподіляються поблизу зон середніх аномалій швидкості/високих аномалій V_P/V_S. Подібні зони швидкості й співвідношення V_P/V_S, нанесені на карту, відповідають даним багатьох попередніх геофізичних досліджень під Південно-Східною Анатолією, зокрема, низьким швидкостям P_n- і S_n-хвиль, високою швидкості загасання, S_n-хвиль високому тепловому потоку тощо. Результати, отримані під цим регіоном Анатолійського плато, також подібні до даних щодо інших континентальних плато, таких як Тибет, і вказують на гарячу, частково розплавлену верхню мантію.

Ключові слова: Південно-Східна Анатолія, структура кори, сейсмічна томографія, структура сейсмічної швидкості, співвідношення V_P/V_S.

Introduction. Southern Turkey, a part of the long Alpine-Himalayan Orogenic Belt (AHOB), suffers from ongoing differential impingement of Arabia and Africa into the weak Anatolian collisional complex which results from the subduction of the Neotethyan Ocean along the Cyprus Arc [e.g., Reilinger and McClusky, 2011]. This coupling has produced one of the most complex crustal interactions along the AHOB. Several major transform faults with distinctive motions, including the northward extension of the Dead Sea Fault zone (DSF), meet in this region [Tatar et al., 2004]. Southeast (SE) Anatolia, the target area of this study, is situated at the junction between the Arabian plate to the southeast, the African plate to the southwest, and the northerly-located Anatolian plate (Fig. 1, *a*). It contains a number of tectono-magmatic/ stratigraphic units as, for example, the metamorphic massifs, the volcanic arc units, granitoid rocks, and the ophiolites [Karaoğlan et al., 2013]. In addition, intrusive and extrusive volcanic igneous (and associated sedimenta-
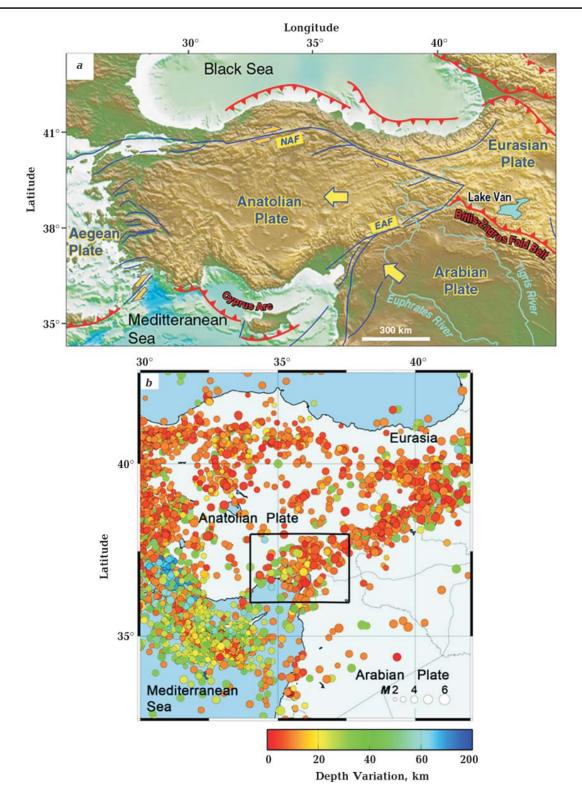
Fig. 1. Tectonic elements at the northeast Mediterranean comprising the Anatolian, Eurasian, and Arabian plates with their complex interactions (from [Schmincke et al., 2014]) (*a*). Tectonic elements partly after [Taymaz et al., 2007]. NAF — North Anatolian Fault; EAF — East Anatolian Fault; DSF — Dead Sea Fault Zone. The yellow arrows point to the direction of the motion of the Arabian and Anatolian plates. Seismicity of the Eastern Mediterranean, Cyprus and the Anatolian plate from the U. S. Geological Survey catalogs (http://earthquake.usgs.gov/earthquakes/search/1976-2014) (*b*). Circles vary in size according to magnitude and in color according to focal depth. The black rectangle shows the present study area.

ry) rocks are reported in SE Anatolia [Robertson et al., 2006, 2007]. Continental collision along the Bitlis-Zagros suture zone began in the early Miocene [Dewey et al., 1973; Dewey, Şengör, 1979] and lead to the westward extrusion of the Anatolian block between two prominent strike slip fault zones [Rotstein, Kafka, 1982], the left-lateral East Anatolian fault zone (EAFZ), and the right-lateral North Anatolian fault zone (NAFZ). The NAFZ is a prominent tectonic feature in northern Anatolia with a confirmed history of seismicity [Öztürk, 2011]. The EAFZ is almost 550 km long, approximately northeast-trending, sinistral strike-slip fault zone comprising a group of faults arranged parallel, subparallel, or even obliquely to the general trend [Öztürk, Bayrak, 2012]. These two fault zones form parts of the boundary between the Anatolian and the Eurasian plates, and between the Arabian and African plates [Westaway, 1994]. The eastern Turkey crust and part of the Lesser Caucasus is hot and weak, and composed of crustal blocks that are in relative motion to one another [Al-Damegh et al., 2005]. The EAFZ joins the NAFZ at the Karliova triple junction north of the Arabian plate, and marks the boundary between Arabia and Anatolia [Nocquet, 2012].

While rotating anticlockwise, the Anatolian plate is also affected by approximately N-S and NNE-SSW shortening induced by the collision between the African and Anatolian plates along the Cyprean arc [Şengör, 1979; Rotstein, 1984; Şengör et al., 1985; Tatar et al., 1995; Bozkurt, Koçyiğit, 1996; Barka, Reilinger, 1997; Reilinger et al., 1997; Tan et al., 2014]. The seismic activity is widely distributed in most parts of the northeast Mediterranean; but highly intense along the active segments of the NAFZ, EAFZ, the Cyprian Arc, and western Anatolia (Fig. 1, *b*), with often many moderate and frequent major events. This notable seismic activity is closely related to the active tectonics in the region [e.g., Tsapanos et al., 2014]. The majority of earthquakes in the northeastern Mediterranean are shallow with some intermediate-depth events along the Cyprian Arc. Overall, complex tectonic activity is responsible for in-tense earthquake activity, deformation, different types of faulting mechanisms, tsunamis, volcanism and geological structures in the Eastern Mediterranean [Yolsal-Çevikbilen, Taymaz, 2012].

Using seismic tomography techniques, scientists decode the information contained in seismograms' squiggles to develop images of individual slices through the deep Earth. These images are used to understand not only the composition of Earth's interior, but also to help explain geologic mysteries like concealed structures, interstitial fluids, earthquake nucleation zones, composition of rocks at the crust-mantle transition, different types of crust-mantle boundary, as well as many other geological processes (see a review by [Zhao, 2001; Janik et al., 2007, 2009; Janik, 2010]). The crustal and upper mantle structures beneath some parts in Anatolia have been studied recently by seismic tomography on different scales [e.g., Sandvol et al., 2001; Nakamura et al., 2002; Al-Lazki et al., 2003, 2004; Bariş et al., 2005; Lei, Zhao, 2007; Salah et al., 2007, 2011, 2014a,b; Schmid et al., 2008; Gans et al., 2009; Koulakov et al., 2010; Mutlu, Karabulut, 2011; Bakırcı et al., 2012; Warren et al., 2013]. However, there is no detailed study dealing with both the compressional- and shear-wave velocities (V_P and V_S, and consequently their V_P/V_S ratio) of the northeastern tip of the Mediterranean including the northwestern corner of the Arabian plate and the southeastern part of the Anatolian plate. Recently, the *P*-wave data set from the local events used in this study, along with teleseismic *P*-wave travel time residuals were used jointly to study the lithospheric structure beneath SE Anatolia [Salah, 2017]. In the present work, we use both the *P*- and *S*-wave arrival times generated by local earthquakes to study the three-dimensional (3D) crustal velocity and V_P/V_S structures of this region. Then, we relate the obtained V_P, V_S, and V_P/V_S models with the available geological and geophysical investigations at SE Anatolia.

Data and Methods. A total of 7132 events which occurred during the period from 2007 to 2012 between latitudes 36,0—38,0° N and longitudes 34—37.6° E was initially collected

for the present study as explained in [Salah, 2017]. These events were recorded by 41 seismic stations operated by different seismic networks in Turkey, including the EDR-Republic of Turkey Prime Ministry, Disaster and Emergency Management Presidency, National Seismological observation network, and the DAF-TUBITAK (The Scientific and Technology Research Council of Turkey). The routine determination of hypocentre parameters is conducted using the crustal model of [Herrin, 1968] and the HYPO71 source code [Lee, Lahr, 1972]. However, the majority of events have focal depths of 7—8 km and the errors in their epicentre locations are relatively large. These location uncertainties are reflected in the large value of the travel-time residual obtained after initial tomographic inversion of the original data set. For this reason, we first relocated the crustal events using an adopted initial 1D P-wave velocity model of 5,8, 6,1, and 6,5 km/s for depths above 5, 18, 42 km, respectively. The Moho is set at a depth of 42 km with a P-wave velocity (V_P) of 7.78 km/s for the uppermost mantle (e.g., [Mooney et al., 1998]). A V_P/V_S ratio of 1.73 is used to obtain the initial S-wave velocity model (Fig. 2). This velocity model is in general agreement with many previous results in and/or close to the study region (e.g., [Horasan et al., 2002;
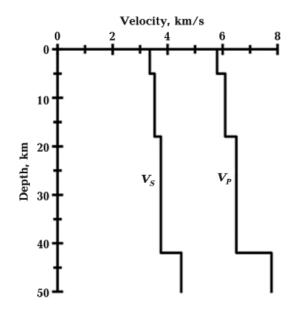
Erduran et al., 2007; Bilim, 2011]). After relocation, we removed all the poorly-located events, thus, the number of local earthquakes is greatly reduced to 2130 [Salah, 2017]. Each event is recorded at a minimum of 6 seismic stations and the errors in the focal depths of all events are lower than 6 km. These 2130 local events produced 13690 and 12560 P- and S-wave arrival times, respectively, recorded by 41 seismic stations. Before relocation, some events were located in the uppermost mantle with focal depths upto 90 km. Due to the uncertainty associated with these events, they were excluded from the final tomograph inversion. The accuracy of arrival times is estimated to be lesser than 0,12 s for P-wave data and less than 0,18 s for S-wave data. The majority of the local earthquakes are located in the central and eastern parts of the study area with prominent concentration along the active segments of the EAFZ. The seismic stations, on the other hand, are uniformly distributed in the land portion located in SE Anatolia and northwest Arabia (refer to [Salah, 2017] for more details). This distribution pattern affects the spatial resolution and reliability of the obtained velocity structures.

To invert the local arrival time data in SE Anatolia for a 3D seismic velocity structure (δV_P and δV_S), we used the tomographic method of [Zhao et al., 1992, 1994, 2012]. A 3D grid net, with the proper spacing, is set up in the model to express the 3D velocity structure. A grid spacing of 0,33° in horizontal directions is adopted for the present study (Fig. 3, *a*). Four layers of grid nodes in the vertical direction, on the other hand, are set up at 10, 22, 36, and 55 km depths (Fig. 3, *b*). We used the initial P-wave velocity model described before (See Fig. 2) for the tomograph inversion, whereas the initial S-wave velocity model is calculated using a V_P/V_S ratio of 1,7296, which is derived from the Wadati diagram constructed using the whole data sets [Salah, 2017]. The different layers were assigned the given V_P values which are constant within an individual layer but change at the boundaries between the layers. These, finally-adopted, initial velocity models give the minimum root-mean-square (RMS) travel time residuals when used
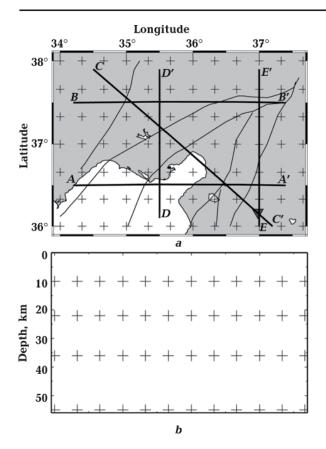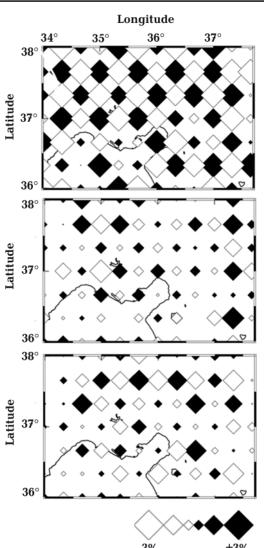
Fig. 2. The adopted initial P- and S-wave velocity models used in the relocation of events (see text for details).

Fig. 3. Configuration of the grid net adopted for the present study in horizontal (*a*) and depth (*b*), directions. The grid spacing is 0,33° and 6—20 km in horizontal and depth directions, respectively. Straight lines in (*a*) denote the location of five vertical cross sections shown later. Black lines denote active faults. Inverted red triangle denotes the Holocene Kilis volcano.

as starting models for the final tomographic inversion. Before adopting these initial V_P and V_S models, we tested slightly different models by changing the velocities within the limits of ±5 % and noticed that the changes in the final velocity structures are very low and does not exceed 1 % from each other.

After computing the *P*- and *S*-wave velocity models we calculated the V_P/V_S ratio at the different crustal layers. This ratio (or the Poisson's ratio) is more significant in characterizing the petrophysical properties of crustal rocks and provides better constraints on the crustal composition and interstitial fluids than the seismic wave velocities (e.g., [Christensen, 1996; Zhao et al., 2004; Bariş et al., 2005; Salah et al., 2007, 2011; Janik, 2010]). Based on the NEIC (the National Earthquake Information Center, USGS) catalogs, we found a total of 12

moderate/large crustal events (M_b or M_w≥5,0) that occurred in the study area since 1979. We plot the epicenters of these events on the obtained velocity and V_P/V_S anomalies to characterize the seismogenic zones in the area.

Resolution and results. One of the well-established and straightforward methods to assess the reliability of the obtained velocity models is the checkerboard (CKB) resolution test (e.g., [Zhao et al., 1992]). Synthetic velocity anomalies of ±3 %, whose image is straightforward and easy to remember, are alternatively assigned to the 3D grid nodes in order to generate a checkerboard pattern. The corresponding synthetic arrival times are then calculated for this input model. Stations locations, event numbers and locations, and accordingly ray paths, in the synthetic data are the same as those in the real data. Random errors of similar magnitude to those of the real data are also added to the synthetic arrival times and are then inverted with the same tomographic method. The inverted image of the checkerboard distinguishes between areas of good and poor resolution. Figs. 4 and 5, display the resulting images of both the δV_P and δV_S structures, respectively, at three crustal layers. The CKB test points to a good and uniform resolution of about 35 km horizontally for the two data sets. Due to the scarce distribution of both the seismic events and the recording stations in the southern and western parts of the study area, the resolution of the obtained velocity images at these areas, especially those at a depth of 36 km, is relatively poor (See Fig. 5).

Adopting the tomographic method described in section two to the SE Anatolia data set, we found that the sum of squared travel-time residuals was reduced by more than 50 % of its initial value. We conducted a number of tomograph inversions using different values for the damping and generated a trade-off curve of the norm of the solution versus the final RMS travel-time residual (Fig. 6). Considering the balance between the reduction of travel time residuals and the smoothness of the obtained velocity model, a damping value of 8 was selected as the best damping for the present tomograph inversion and regulariza-

Fig. 4. Results of the checkerboard resolution test for *P*-wave velocity at three crustal depths (see text for details). Black and white rhombs denote high and low velocities, respectively. The perturbation scale (±3 %) is shown at the bottom. The depth of each layer is shown below every map.
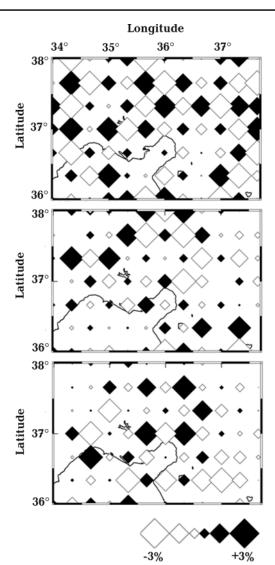
Fig. 5. Results of the checkerboard resolution test for *S*-wave velocity at three crustal depths. Other details are similar to those of Fig. 4.
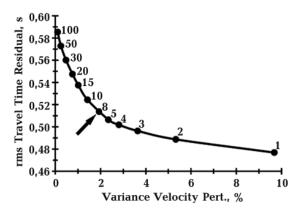

Fig. 6. Trade-off curve of the variance velocity perturbation (%) and the root-mean-square travel time residual at different values of the damping parameter (numbers on the curve). A pen pointing to the best damping is shown at a value of 8.

tion. The final RMS travel time residuals are 0,34 s and 0,46 s for the *P*-wave, and *S*-wave data sets, respectively. Significant parts of the study area have enough ray coverage at the three depth layers (10, 22, and 36 km) in which the number of *P* and *S* rays hitting each grid node is adequate to retrieve the velocity structures (Figs. 7 and 8). Although the two 22 and 36 km depth layers are assigned the same initial velocity values (See Fig. 2), we expect different final velocity structures because the velocity at any point in the model is calculated by linear interpolation of the eight surround-
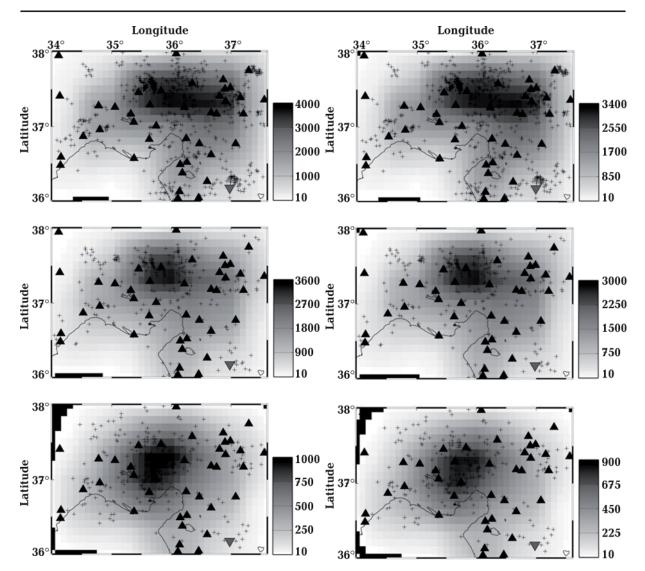
Fig. 7. Number of rays passing through each grid node (hit count) for *P*-wave data at three depth slices. Grid nodes with rays <8, and consequently poor coverage are not included in the tomographic inversion.
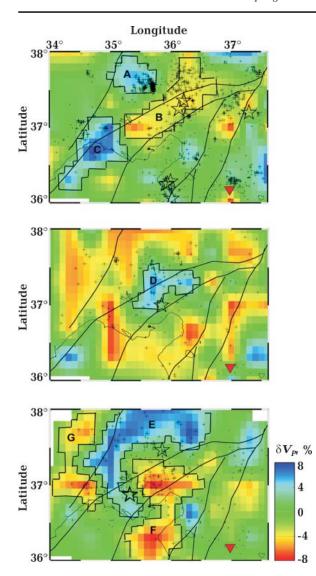
Fig. 8. Number of rays passing through each grid node for *S*-wave data at three depth slices. Other details are similar to those of Fig. 7.

ing grid nodes in the horizontal and vertical directions [Zhao et al., 1992]. Grid nodes of less than 10 rays are not included in the final tomograph inversion. It is clear that the central, eastern and northeastern parts have large hit counts and many nodes are hit by more than 4000 rays at the first two crustal layers.

Inversion results of δV_P, δV_S, and V_P/V_S distributions in map views at three crustal layers are shown, respectively, in Figs. 9, 10, and 11. In addition, Figs. 12—16 show the δV_P, δV_S, and V_P/V_S images along five vertical cross-sections in SE Anatolia (refer to Fig. 3 for the location of cross-sections). The veloc-

ity images show the velocity perturbations in percentage from the initial velocity model at each depth slice or cross section. Although some researchers present absolute velocities which increase generally with depth (e.g., [Hearn, Ni, 1994; Al-Lazki et al., 2004]), displaying velocity perturbations (%) are much more preferred as they show clearly and easily areas of high or low velocity anomalies (e.g., [Zhao et al., 1992, 1994]).

Significant lateral and vertical variations of up to ±8 % of velocity (δV_P and δV_S) and V_P/V_S ratio are revealed in the study area. Higher V_P zones are visible at the upper crust beneath the western side, in the central part
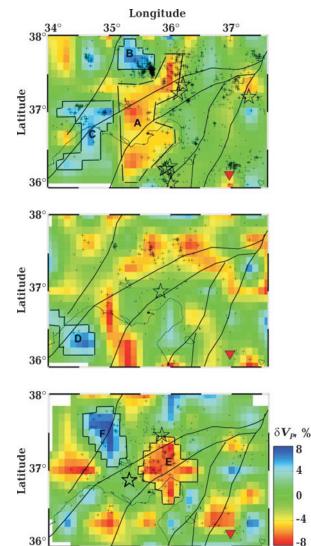
Fig. 9. *P*-wave velocity structures (in %) at three depth slices beneath southeast Anatolia. Red and blue colors denote low and high velocities, respectively. Numbers between brackets show the depth range of the micro-seismic activity plotted as crosses. Moderate and large earthquakes (*M*≥5,0) in the same depth range of the background seismicity are plotted as red stars. Thin solid lines denote active faults in southeast Anatolia. Inverted red triangles denote the Holocene Kilis volcano. The perturbation scale (±8 % for the shallowest layer and ±7 % for the remaining) is shown to the lower right.

Fig. 10. *S*-wave velocity structures at the three depth slices. Other details are similar to those of Fig. 9.

at middle crust, and in the central northern regions at the lower crust (See Fig. 9, anomalies A, C, D and E). These high-velocity areas might represent asperities of highly consolidated rocks. Lower-than-average V_P anomalies, on the other hand, are revealed at many parts at middle crustal depths and in broad zones at both the upper and lower crust (See

Fig. 9, anomalies B, F, and G). A clear, low shear wave velocity anomaly is clearly visible at a depth of 10 km in the central part of the study area (See Fig. 10, *a*, anomaly A). Another prominent low shear wave velocity anomaly can also be seen at a depth of 36 km (See Fig. 10, *c*, anomaly E). A number of low V_S anomalies to the south and west are also visible at this depth. The magnitude of the low-velocity anomalies is larger near the EAFZ and the Holocene volcano at the southeast (See Figs. 9, *b*, *c* and 10, *b*, *c*). High V_S zones to the west of the study area at both the upper and lower crust are also imaged (See Fig. 10, anomalies B, C, D, and F). In addition, most
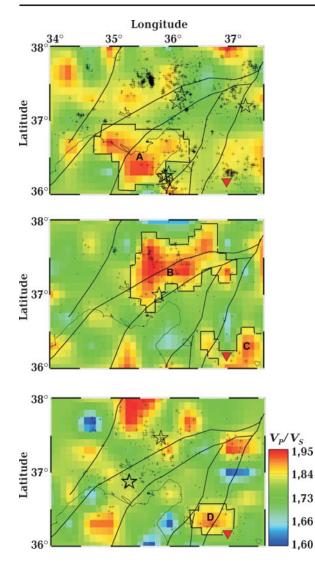
Fig. 11. Distribution of V_P/V_S structures at three depth slices. Red and blue colors denote high and low V_P/V_S ratio, respectively. The variation scale (1,60—1,95) is shown to the lower right. Other details are similar to those of Fig. 9.

Fig. 12. Vertical cross sections of δV_P, δV_S and V_P/V_S structures along line AA' (see Fig. 3 for the location of the cross sections). The red color denotes low velocity and high V_P/V_S ratio; whereas high velocities and low V_P/V_S ratios are shown in blue. Crosses show the location the microseismic activity in a 40 km-wide-zone around the profile. The perturbation scales (±7 % for velocity and 1,60—1,95 for V_P/V_S ratio) are shown to the right.

of the microseismic activity is concentrated along the EAFZ and to some heterogeneous zones of low- to average-velocity anomalies. The background seismicity is scarce along the strong asperities implying that such areas are capable of resisting accumulated stress.

The V_P/V_S ratio varies between around ±7,5 % and hence, shows a high structural heterogeneity at the different crustal layers (See Fig. 11, anomalies A and B). It is generally higher than 1,73 at all depth slices, implying a general low S-wave velocity structure compared to the P-wave velocity. Prominent high V_P/V_S anomalies are evident beneath
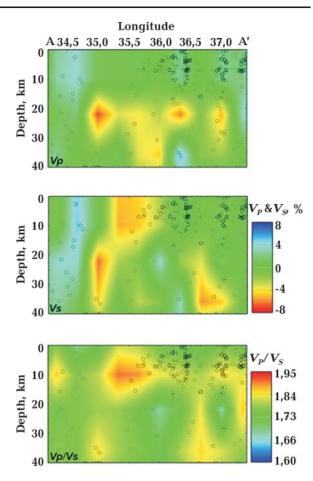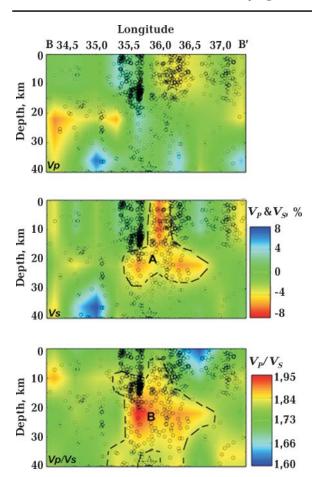
the active volcano in the south (See Fig. 11, anomalies C and D), and along the active segments of the EAFZ. A number of high V_P/V_S zones are also distributed in the lower crust (See Fig. 11, *c*). These areas may represent the conduits for the vertically ascending hot fluids from the uppermost mantle beneath the study area. All the moderate/large earthquakes are located in areas characterized by low/average velocity and average/high V_P/V_S (See Figs. 9—11). Microseismic activity, on the other hand, is intense in the central and eastern parts of the study area, which are characterized by highly heterogeneous velocity and V_P/V_S ratio structures. Both low veloc-

Fig. 13. Vertical cross sections of δV_P, δV_S and V_P/V_S structures along line BB'. Large stars show the location of moderate-large earthquakes ($M \geq 5,0$) in a 40 km wide-zone around the profile. Other details are similar to those of Fig. 11.

Fig. 14. Vertical cross sections of δV_P, δV_S and V_P/V_S structures along line CC'. Other details are similar to those of Fig. 11.

ity and high V_P/V_S anomalies are clearly visible along the vertical cross sections AA'—EE' (See Figs. 12—16). Prominent, low V_S/high V_P/V_S anomalies are visible along cross section BB' (which correspond to anomalies A and B; Fig. 11). The seismic activity is concentrated in low-velocity/high V_P/V_S zones (See Figs. 13, 15). Another clear low V_S zone is evident at the middle and upper crust along cross section DD' (See Fig. 15, anomaly A). This zone is characterized by high V_P/V_S ratios (See Fig. 15, anomaly B). Lower seismic wave velocities are also visible along cross section EE' with a high V_P/V_S anomaly at lower/middle crustal depths (See Fig. 16). Background seismicity and large crustal earthquakes occur in heterogeneous zones characterized by low-velocity/high V_P/V_S anomalies (See Figs. 13,
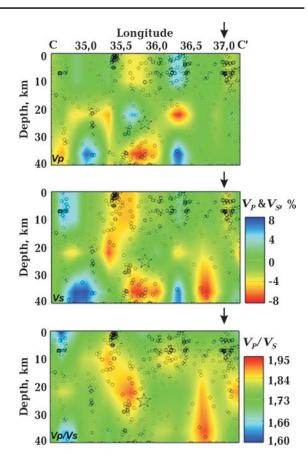
15, 16). Although the *P*-wave velocity is close to its average value at lower crustal depths beneath the Holocene volcano in the southeast; low V_S and high V_P/V_S anomalies are clearly visible beneath the volcano, although shifted slightly to the west (See Figs. 14, 16).

Discussion. ***Previous seismological observations.*** The results of many previous geophysical investigations at SE Anatolia indicate that the region is characterized by heterogeneous structures and complex seismotectonic setting. This is evident from the obtained tomographic images dominated by average- to low-velocity and average to high V_P/V_S anomalies which arise mainly from the extensive faulting, widespread magmatism, and the existence of sedimentary basins in the study area (e.g., [Jaffey et al., 2004]). Hearn and Ni [1994] previously detected low P_n velocity of about 7,8 km/s beneath the Anatolian plate, whereas Rodgers et al. [1997] documented
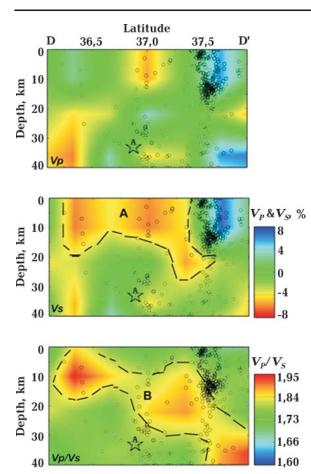
Fig. 15. Vertical cross sections of δV_P, δV_S and V_P/V_S structures along line DD′. Other details are similar to those of Figs. 11 and 12.

Fig. 16. Vertical cross sections of δV_P, δV_S and V_P/V_S structures along line EE′. Other details are similar to those of Figs. 11 and 12.

an inefficient S_n propagation, low P_n velocity, and volcanism indicating possible partial melt in the upper mantle beneath Turkey. Large-scale (~500 km) zones of low (<8 km/s) P_n velocity anomalies were mapped beneath the Anatolian plate and the Anatolian plateau by Al-Lazki et al. [2004] and Al-Damegh et al. [2004]. These are thought to be hot and unstable mantle lid zones, and may partially result from the subduction of the Tethyan oceanic lithosphere beneath Eurasia. A region of very low P_n velocities (<7,8 kms^{-1}) is imaged east of the central Anatolian fault zone, with a transition to faster velocities (>8,1 kms^{-1}) west of the fault [Gans et al., 2009]. These anomalies are also consistent with the heterogeneous P_n structures across Turkey [Mutlu, Karabulut, 2011] with widely distributed low P_n velocities beneath SE Anatolia (east of 35°E). The lowest P_n velocities coincide with the volcanics
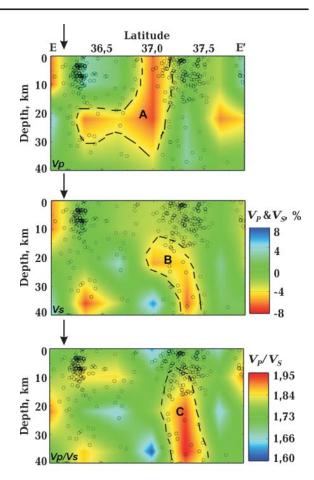
in eastern Anatolia and the central Anatolian volcanic zone. Erduran et al. [2007] detected shallow, very low shear wave velocity of 2,2 km/s that increases to 3,6 km/s at a depth of 10 km beneath Anatolia. They reached to the conclusion that the estimated velocities in almost all depth ranges are significantly lower than the PREM values. In addition, the uppermost mantle beneath the Anatolian plate is represented by a relatively low shear wave velocity of 4,27 km/s. Anomalously low shear wave velocities are found underneath the Anatolian block and the Anatolian plateau in eastern Turkey [Gök et al., 2007; Warren et al., 2013] throughout the whole crust. In addition, recent results of Delph et al. [2015] show that the overall shear wave velocities of the Anatolian crust are low. These low velocities point to upwelling of hot materials from an underlying hot asthenosphere (e.g., [Jiang
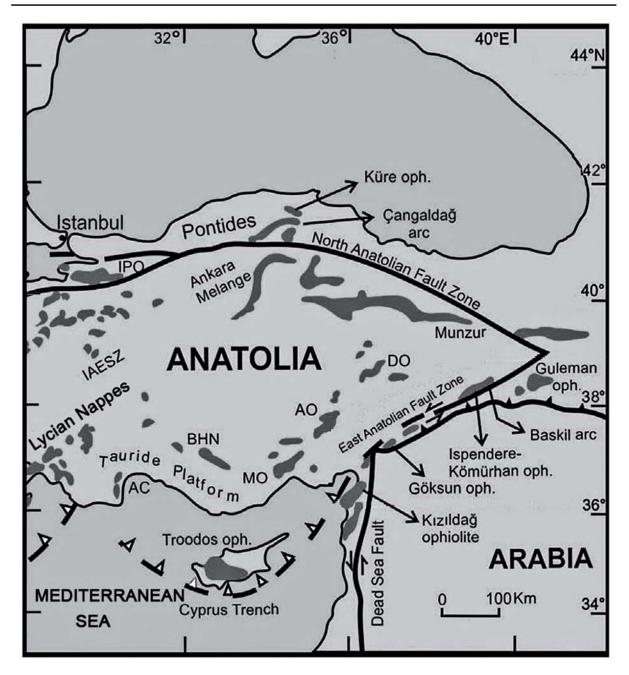
Fig. 17. Distribution of the Neotethyan ophiolites superimposed on the major tectonic features in the eastern Mediterranean region (from [Dilek, Flower, 2003]). AC — Antalya complex; IPO — Intra pontide ophiolites; BHN — Beyşehir-Hoyran nappes; IAESZ — Izmir-Ankara-Erzincan suture zone; MO — Mersin ophiolite; AO — Aladağ ophiolite; DO — Divriği ophiolite.

et al., 2015]). The recent study of Bakırcı et al. [2012] points to a deep source for these low shear-wave velocities. Low S_n velocity of 4,3—4,5 km/s [Gök et al., 2003; Tezel et al., 2007], and upper mantle low *P*-wave velocities [Lei, Zhao, 2007] detected beneath eastern Anatolia support this hypothesis. These low velocity anomalies are probably related to the absence of a lithospheric mantle lid and its replacement with asthenospheric materials. Inversion results of Tezel et al. [2007] indicate that the Anatolian region has a shallow low shear-wave velocity zone at 7—20 km depths, which are consistent with the low shear wave velocity anomalies detected at a depth of 10 km (See Figs. 9, *b*, 12, 14—16).

High attenuation (low Q) zones beneath different parts of Anatolia have been detected by many researchers [Zor et al., 2007; Pasyanos et al., 2009]. Lower values of $L_g Q_0$ were also detected recently by Kaviani et al. [2015] over the Turkish-Anatolian plateau (<150) than those observed over the Iranian plateau (150—400).

The ophiolites and their associated low-velocity/high V_P/V_S ratio. The ophiolites of SE Anatolia occur in two main belts, namely the Peri-Arabic belt and the SE Anatolian ophiolites (Fig. 17). The former were extruded directly onto the Arabian platform; whereas the latter were tectonically emplaced beneath the Tauride platform and cut by calc-alkaline volcanic granitoid rocks [Karaoğlan et al., 2013]. The ophiolites in the two belts exhibit a complete ophiolite pseudostratigraphy and are geochemically classified as suprasubduction zone (SSZ) type (for more details, refer to [Parlak et al., 2004; Bağci et al., 2005, 2006, 2008]). Studies of [Parlak et al., 2009] on the petrology and geochemistry of Neotethyan ophiolites point also to extensive distribution of Late Cretaceous ophiolitic belts running NE-SW; almost parallel to the orientation of the EAFZ (in our study area, these are the MO-AO-DO and the EAFZ trends). It is well known that the presence of serpentine and other hydrous minerals have significant effects on the physical and mechanical properties of crustal and upper mantle rocks, including a decrease in seismic velocity, an increase in Poisson′s ratio, generation of seismic reflectivity, an increase in magnetization, a reduction in density, an increase in electrical conductivity, and reduction in mechanical strength (e.g., [Christensen, 1978; Horen et al., 1996]). Extensive research of Christensen [1966, 1978] showed that original V_P/V_S values of 1,76—1,81 may increase to 1,87 at 15 % serpentinization and even to 2,27 at 100 % serpentinization. High V_P/V_S values between 1,75—1,83 indicate a composition of intermediate to mafic rocks [Paswan et al., 2016]. The widely distributed high V_P/V_S zones in our results at the upper/middle crustal depths (See Fig. 11, anomalies A, and B) are consistent with the MO-AO-DO trend in SE Anatolia

[Dilek, Flower, 2003; Karaoğlan et al., 2013] (See Fig. 17). In addition, high V_P/V_S zones at middle/lower crustal depths (See Fig. 11, anomalies C and D) are mapped near the Holocene volcano. Low seismic wave velocities are also seen parallel to the two ophiolite trends discussed above (for example anomalies B and F in Fig. 9, and anomalies A and E in Fig. 10).

Other geophysical investigations. The Curie point depths estimated by Bektaş et al. [2007] over the region indicate generally high temperatures within the crust and a possibly demagnetized lower crust. The presence of hot springs (>45 °C) and the young-aged volcanic rocks in the region support these anomalously high temperatures. These observations suggest that the uppermost mantle and perhaps parts of the overlying lower crust are partially molten and the asthenosphere is close to the base of the crust; both of which are consistent with the existence of the volcanism in the region. Hartlap hot spring located at 37,53° N and 36,67° E, with a water temperature of up to 37 °C, in the northeast part of the study area only few kilometers to the north of the EAFZ, is related to the faulting system in Inner East Anatolia [Bektaş, 2013]. It is, however, believed that the mantle heat flow in the region may not have made its way to the surface. Instead, it is too deep to heat the hot springs generally found in Inner East Anatolia [Bektaş, 2013].

Conclusions. In addition to more detailed V_P structures compared to the results of Salah (2017), the present study provides fine shear wave velocity and V_P/V_S structures beneath SE Anatolia which are determined by inverting a number of P- and S-wave arrival times generated by local earthquakes recorded at 41 seismic stations. Results of the checkerboard resolution test and hit counts imply that the mapped structures are real down to the depth of the Moho discontinuity. The following points outline the main conclusions of the present study.

1. The crustal velocity structure is highly inhomogeneous and contains many lower-than-average velocity anomalies. The low-velocity zones are more widely distributed

beneath the active faults and areas of thick sedimentary cover.

2. Distinct high V_P/V_S structures are clearly seen at all depth slices, which might be related to the presence of partial melt in the lower crust and the uppermost mantle. The high V_P/V_S areas are consistent with the existence of ophiolite belts.

3. Although some events occur in high seismic velocity zones; most of the large crustal earthquakes are found in average/low velocity and average/high V_P/V_S anomalies. This indicates that the large crustal events occur away from weak areas that may deform aseismically, but not in those characterized by higher-than-average velocity, which are capable of resisting relatively large stresses.

SE Anatolia is an area that is characterized by the presence of some sedimentary basins, extensive faulting, ophiolite belts, and Cenozoic volcanics. The presently mapped low-velocity/high V_P/V_S zones are in agreement with such circumstances. Many previous geophysical observations such as low P_n and S_n velocities, high S_n attenuation, high heat flow, low $L_g\,Q_0$ values, and high geothermal potential support the imaged low-velocity/high V_P/V_S ratio zones. The results of these geophysical observations beneath southeast Anatolia are analogous to other continental plateaus such as the Tibet and are interpreted to be an indication of a serpentinized hot mantle that could be partially molten. The presence of this partial melt in the uppermost mantle feeds the widespread Cenozoic volcanism in the Anatolian plateau.

3D crustal velocity and V_P/V_S structures beneath Southeast Anatolia and their geodynamic implications

M. K. Salah, Ş. Şahin, 2019

We applied a seismic tomography method to arrival time data generated by local crustal earthquakes in Southeast Anatolia to study the shallow, three-dimensional, velocity and V_P/V_S structures beneath the area. Many of the previous seismological studies of the region are of a regional, or even global, scale. A total of 2150 carefully-selected events generating 13690 and 12560 P- and S-wave arrival times are finally used in the tomographic inversion. Results of the checkerboard resolution test imply that the obtained velocity and V_P/V_S anomalies are reliable features. In addition, hit count maps indicate that all parts are hit by an adequate number of rays to retrieve the crustal velocity structure. Strong lateral crustal heterogeneities are revealed beneath southeast Anatolia with many lower-than-average velocity anomalies. The low velocity anomalies are imaged especially near the active fault segments. In addition, high V_P/V_S ratios are mapped at most crustal layers especially at depths of 10 and 22 km which are consistent with the distribution of ophiolite belts. The high V_P/V_S zones are induced by the possible existence of over-pressurized fluids in the crust and perhaps the uppermost mantle. The existence of these fluids along with the intense tectonic activity could trigger large crustal earthquakes along the western segment of the East Anatolian fault zone. Although may occur in high velocity zones, the majority of the large crustal earthquakes are distributed near zones of average velocity/high V_P/V_S anomalies. Such mapped velocity and V_P/V_S zones are in agreement with many previous geophysical investigations beneath southeast Anatolia such as low P_n and S_n velocities, high S_n attenuation, high heat flow, and low $L_g\,Q_0$ values. Results beneath this region of the

Anatolian Plateau are also similar to those observed beneath other continental plateaus such as the Tibet and point to a hot, partially-molten upper mantle.

Key words: Southeast Anatolia, crustal structure, seismic tomography, seismic velocity structure, V_P/V_S ratio.

References

Al-Damegh, K., Sandvol, E., Al-Lazki, A., & Barazangi, M. (2004). Regional seismic wave propagation (*Lg* and *Sn*) and *Pn* attenuation in the Arabian plateau and surrounding regions. *Geophysical Journal International, 157*(2), 775—795. https://doi.org/10.1111/j.1365-246X.2004.02246.x.

Al-Damegh, K., Sandvol, E., & Barazangi, M. (2005). Crustal structure of the Arabian plate: new constraints from the analysis of teleseismic receiver functions. *Earth and Planetary Science Letters, 231*(3-4), 177—196. doi: 10.1016/j.epsl.2004.12.020.

Al-Lazki, A. I., Sandvol, E., Seber, D., Barazangi, M., Turkelli, N., & Mohamad, R. (2004). *Pn* tomographic imaging of mantle lid velocity and anisotropy at the junction of the Arabian, Eurasian and African plates. *Geophysical Journal International, 158*(3), 1024—1040. doi: 10.1111 /j.1365-246X.2004.02355x.

Al-Lazki, A. I., Seber, D., Sandvol, E., Turkelli, N., Mohamad, R., & Barazangi, M. (2003). Tomographic *Pn* velocity and anisotropy structure beneath the Anatolian plateau (eastern Turkey) and surrounding regions. *Geophysical Research Letters, 30*(24), 8043. doi: 10.1029/2003GL017391.

Bağci, U., Parlak, O., & Höck, V. (2005). Whole rock and mineral chemistry of cumulates from the Kızıldağ (Hatay) ophiolite (Turkey): clues for multiple magma generation during crustal accretion in the southern Neotethyan Ocean. *Mineralogical Magazine, 69*(1), 53—76. https://doi.org/10.1180/0026461056910234.

Bağcı, U., Parlak, O., & Höck, V. (2006). Geochemical character and tectonic environment of ultramafic to mafic cumulates from the Tekirova (Antalya) ophiolite (Southern Turkey). *Geological Journal, 41*(2), 193—219. https://doi.org/10.1002/gj.1035.

Bağci, U., Parlak, O., & Höck, V. (2008). Geochemistry and tectonic environment of diverse magma generations forming the crustal units of the Kızıldağ (Hatay) ophiolite, Southern Turkey. *Turkish Journal of Earth Sciences, 17*, 43—71.

Bakırcı, T., Yoshizawa, K., & Özer, M. F. (2012). Three-dimensional *S*-wave structure of the upper mantle beneath Turkey from surface wave tomography. *Geophysical Journal International, 190*(2), 1058—1076. doi: 10.1111/j.1365-246X.2012.05526.x.

Bariş, Ş., Nakajima, J., Hasegawa, A., Honkura, Y., Ito, A., & Üçer, S. B. (2005). Three-dimensional structure of V_P, V_S, and V_P/V_S in the upper crust of the Marmara region, NW Turkey. *Earth, Planets and Space, 57*(11), 1019—1038. https://doi.org/10.1186/BF03351882.

Barka, A. A., & Reilinger, R. (1997). Active tectonics of the eastern Mediterranean region deduced from GPS, neotectonic, and seismicity data. *Annali di Geofisica, 40*, 587—610.

Bektaş, Ö. (2013). Thermal structure of the crust in Inner East Anatolia from aeromagnetic and gravity data. *Physics of the Earth and Planetary Interiors, 221*, 27—37. http://dx.doi.org/10.1016/j.pepi.2013.06.003.

Bektaş, Ö., Ravat, D., Büyüksaraç, A., Bilim, F., & Ateş, A. (2007). Regional geothermal characterization of East Anatolia from aeromagnetic, heat flow and gravity data. *Pure and Applied Geophysics, 164*(5), 975—998. doi: 10.1007/s00024-007-0196-5.

Bilim, F. (2011). Investigation of the Galatian volcanic complex in the northern central Turkey using potential field data. *Physics of the Earth and Planetary Interiors, 185*(1-2), 36—43. doi: 10.1016 /j.pepi.2011.01.001.

Bozkurt, E., & Koçyiğit, A. (1996). The Carova basin: an active negative flower structure on the Almus fault zone, a splay fault system of the North Anatolian Fault Zone. *Tectonophysics, 265*(3-4), 239—254. https://doi.org/10.1016/S0040-1951(96)00045-5.

Christensen, N. I. (1966). Elasticity of ultrabasic rocks. *Journal of Geophysical Research,*

71(24), 5921—5931. https://doi.org/10.1029/JZ071i024p05921

Christensen, N. I. (1978). Ophiolites, seismic velocities and oceanic crustal structure. *Tectonophysics, 47*(1-2), 131—157. https://doi.org/10.1016/0040-1951(78)90155-5.

Christensen, N. I. (1996). Poisson's ratio and crustal seismology. *Journal of Geophysical Research: Solid Earth,* 101(B2), 3139—3156. https://doi.org/10.1029/95JB03446.

Delph, J. R., Biryol, C. B., Beck, S. L., Zandt, G., & Ward, K. M. (2015). Shear wave velocity structure of the Anatolian Plate: anomalously slow crust in southwestern Turkey. *Geophysical Journal International, 202*(1), 261—276. doi: 10.1093/gji/ggv141.

Dewey, J. F., Pitman, W. C., Ryan, W. B. F., & Bonnin, J. (1973). Plate tectonics and the evolution of the Alpine system. *Geological Society America Bulletin, 84*(10), 3137—3180. https://doi.org/10.1130/0016-7606(1973)84<3137:PTATEO>2.0.CO;2.

Dewey, J., & Şengör, A. (1979). Aegean and surroundings regions: complex multiplate and continuum tectonics in a convergent zone. *Geological Society America Bulletin, 90*(1), 84—92. https://doi.org/10.1130/0016-7606(1979)90<84:AASRCM>2.0.CO;2.

Dilek, Y., & Flower, M. F. J. (2003). Arc-trench rollback and forearc accretion: 2. A model template for ophiolites in Albania, Cyprus, and Oman. In: Dilek, Y. & Robinson, P. T. (Eds.), *Ophiolites in Earth History* (Vol. 218, pp. 43—68). Geological Society of London. Special Publication. https://doi.org/10.1144/GSL.SP.2003.218.01.04.

Erduran, M., Çakir, Ö., Tezel, T., Şahin, Ş., & Alptekin, Ö. (2007). Anatolian surface wave evaluated at GEOFON station ISP Isparta, Turkey. *Tectonophysics,* 434(1-4), 39—54. https://doi.org/10.1016/j.tecto.2007.02.005.

Gans, C. R., Beck, S. L., Zandt, G., Biryol, C. B., & Özacar, A. A. (2009). Detecting the limit of slab break-off in central Turkey: new high-resolution P_n tomography results. *Geophysical Journal International, 179*(3), 1566—1572. doi: 10.1111/j.1365-246X.2009.04389.x.

Gök, R., Sandvol, E., Turkelli, N., Seber, D., & Barazangi, M. (2003). S_n attenuation in the Anatolian and Iranian plateau and surrounding regions. *Geophysical Research Letters, 30*(24), 8042. doi: 10.1029/2003GL018020.

Gök, R., Pasyanos, M. E., & Zor, E. (2007). Lithospheric structure of the continent–continent collision zone: eastern Turkey. *Geophysical Journal International, 169*(3), 1079—1088. doi: 10.1111/j.1365-246X.2006.03288.x.

Hearn, T. M., & Ni, J. (1994). *Pn* velocities beneath continental collision zones: the Turkish-Iranian Plateau. *Geophysical Journal International, 117*(2), 273—283. https://doi.org/10.1111/j.1365-246X.1994.tb03931.x.

Herrin, E. (1968). Seismological tables for *P*-phases. *Bulletin of the Seismological Society of America, 60*, 461—489.

Horasan, G., Gülen, L., Pinar, A., Kalafat, D., Ozel, N., Kuleli, H. S., & Isikara, A. M. (2002). Lithospheric structure of the Marmara and Aegean regions, western Turkey. *Bulletin of the Seismological Society of America, 92*, 322—329. htpp://doi.org/10.1785/0120000813.

Horen, H., Zamora, M., & Dubuisson, G. (1996). Seismic waves velocities and anisotropy in serpentinized peridotites from Xigaze ophiolite: abundance of serpentine in slow spreading ridge. *Geophysical Research Letters, 23*(1), 9—12. https://doi.org/10.1029/95GL03594.

Jaffey, N., Robertson, A., & Pringle, M. (2004). Latest Miocene and Pleistocene ages of faulting, determined by ^{40}Ar/^{39}Ar single-crystal dating of air-fall tuff and silicic extrusives of the Erciyes Basin, central Turkey: evidence for intraplate deformation related to the tectonic escape of Anatolia. *Terra Nova, 16*, 45—53. doi: 10.1111/j.13653121.2003.00526.x.

Janik, T. (2010). Upper lithospheric structure in the central Fennoscandian Shield: constraints from *P*- and *S*-wave velocity models and V_P/V_S ratio distribution of the BALTIC wide-angle seismic profile. *Acta Geophysica, 58*(4), 543—586. doi: 10.2478/s11600-010-0002-0.

Janik, T., Kozlovskaya, E., & Yliniemi, J. (2007). Crust-mantle boundary in the central Fennoscandian shield: Constraints from wide-angle *P*- and *S*-wave velocity models and new results of reflection profiling in Finland. *Journal of Geophysical Research: Solid Earth, 112*(B4), B04302. doi: 10.1029/2006JB004681.

Janik, T., Kozlovskaya, E., Heikkinen, P., Ylini-

emi, J., & Silvennoinen, H. (2009). Evidence for preservation of crustal root beneath the Proterozoic Lapland-Kola orogen (northern Fennoscandian shield) derived from *P*- and *S*-wave velocity models of POLAR and HUKKA wide-angle reflection and refraction profiles and FIRE4 reflection transect. *Journal of Geophysical Research: Solid Earth, 114*(B6), B06308. doi: 10.1029/2008JB005689.

Jiang, G., Zhang, G., Zhao, D., Lüd, Q., Li, H., & Li, X. (2015). Mantle dynamics and Cretaceous magmatism in east-central China: Insight from teleseismic tomograms. *Tectonophysics, 664*, 256—268, http://dx.doi.org/10.1016/j.tecto.2015.09.019.

Karaoğlan, F., Parlak, O., Klötzli, U., Koller, F., & Rızaoglu, T. (2013). Age and duration of intra-oceanic arc volcanism built on a supra-subduction zone type oceanic crust in southern Neotethys, SE Anatolia. *Geoscience Frontiers, 4*(4), 399—408. http://dx.doi.org/10.1016/j.gsf.2012.11.011.

Kaviani, A., Sandvol, E., Bao, X., Rümpker, G., & Gök, R. (2015). The structure of the crust in the Turkish–Iranian Plateau and Zagros using *Lg Q* and velocity. *Geophysical Journal International, 200*(2), 1252—1266. doi: 10.1093/gji/ggu468.

Koulakov, I., Bindi, D., Parolai, S., Grosser, H., & Milkereit, C. (2010). Distribution of seismic velocities and attenuation in the crust beneath the North Anatolian Fault (Turkey) from local earthquake tomography. *Bulletin of the Seismological Society of America, 100*, 207—224. doi: 10.1785/0120090105.

Lee, W. H. K., & Lahr, J. C. (1972). *HYP071: a computer program for determining hypocenter, magnitude, and first motion pattern of local earthquakes.* Open File Report, U. S. Geological Survey, 100 p.

Lei, J., & Zhao, D. (2007). Teleseismic evidence for a break-off subducting slab under eastern Turkey. *Earth and Planetary Science Letters, 257*(1-2), 14—28. doi: 10.1016/j.epsl.2007.02.011.

Mooney, W. D., Laske, G., & Masters, T. G. (1998). CRUST 5.1: A global crustal model at 5°×5°. *Journal of Geophysical Research 103*(B1), 727—747. https://doi.org/10.1029/97JB02122.

Mutlu, A. K., & Karabulut, H. (2011). Anisotro-

pic P_n tomography of Turkey and adjacent regions. *Geophysical Journal International, 187*, 1743—1758. doi: 10.1111/j.1365-246X.2011.05235.x.

Nakamura, A., Hasegawa, A., Ito, A., Üçer, B., Barış, Ş., Honkura, Y., Kono, T., Hori, S., Pektaş, R., Komut, T., Çelik, C., & Işıkara, A. M. (2002). *P*-wave velocity structure of the crust and its relationship to the occurrence of the İzmit, Turkey, earthquake and aftershocks. *Bulletin of the Seismological Society of America, 92*, 330—338.

Nocquet, J.-M. (2012). Present-day kinematics of the Mediterranean: A comprehensive overview of GPS results. *Tectonophysics, 579*, 220—242. doi: 10.1016/j.tecto.2012. 03.037.

Öztürk, S. (2011). Characteristics of seismic activity in the western, central and eastern parts of the North Anatolian Fault Zone, Turkey: temporal and spatial analysis. *Acta Geophysica, 59*(2), 209—238, doi: 10.2478/s11600-010-0050-5.

Öztürk, S., & Bayrak, Y. (2012). Spatial variations of precursory seismic quiescence observed in recent years in the eastern part of Turkey. *Acta Geophysica, 60*(1), 92—118. doi: 10.2478/s11600-011-0035-z.

Parlak, O., Höck, V., Kozlu, H., & Delaloye, M. (2004). Oceanic crust generation in an island arc tectonic setting, SE Anatolian Orogenic Belt (Turkey). *Geological Magazine, 141*(5), 583—603. https://doi.org/10.1017/S0016756804009458.

Parlak, O., Rızaoğlu, T., Bağcı, U., Karaoğlan, F., & Höck, V. (2009). Tectonic significance of the geochemistry and petrology of ophiolites in southeast Anatolia, Turkey. *Tectonophysics, 473*(1-2), 173—187. doi: 10.1016/j.tecto.2008.08.002.

Paswan, A. K., Goyal, A., Kumar, R., & Borah, K. (2016). *Crustal shear velocity structure beneath Cuddapah Basin, India.* Geophys. Res. Abst. 18, EGU2016-PREVIEW.

Pasyanos, M. E., Matzel, E. M., Walter, W. R., & Rodgers, A. J. (2009). Broad-band L_g attenuation in the Middle East. *Geophysical Journal International, 177*(3), 1166—1176. doi: 10.1111/j.1365-246X.2009.04128.x.

Reilinger, R., & McClusky, S. (2011). Nubia-Ara-

bia-Eurasia plate motions and the dynamics of Mediterranean and Middle East tectonics. *Geophysical Journal International, 186*(3), 971—979. doi: 10.1111/j.1365-246X.2011.05133.x.

Reilinger, R. E., McClusky, S. C., Oral, M. B., King, W., & Toksöz, M. N. (1997). Global Positioning System measurements of present-day crustal movements in the Arabian-Africa-Eurasia plate collision zone. *Journal of Geophysical Research: Solid Earth, 102*(B5), 9983—9999. https://doi.org/10.1029/96JB03736.

Robertson, A., Ustaömer, T., Parlak, O., Ünlügenç, U. C., Taslı, K., & İnan, N. (2006). The Berit transect of the Tauride thrust belt, S. Turkey: late Cretaceous-Early Cenozoic accretionary/collisional processes related to closure of the southern Neotethys. *Journal of Asian Earth Sciences, 27*(1), 108—145. https://doi.org/10.1016/j.jseaes.2005.02.004.

Robertson, A. H. F., Parlak, O., Rızaoğlu, T., Ünlügenç, Ü., İnan, N., Taslı, K., & Ustaömer, T. (2007) Tectonic evolution of the South Tethyan ocean: evidence from the Eastern Taurus Mountains (Elazığ region, SE Turkey). In: A. C. Ries, R. W. H. Butler, & R. H. Graham (Eds.), *Deformation of Continental Crust* (Vol. 272, pp. 231—270). Geological Society of London. Special Publication.

Rodgers, A. J., Ni, J. F., & Hearn, T. M. (1997). Propagation characteristics of short-period *Sn* and *Lg* in the Middle East. *Bulletin of the Seismological Society of America, 87*, 396—413.

Rotstein, Y. (1984). Counterclockwise rotation of the Anatolian block. *Tectonophysics, 108*(1-2), 71—91. https://doi.org/10.1016/0040-1951(84)90155-0.

Rotstein, Y., & Kafka, A. (1982). Seismotectonics of the southern boundary of Anatolia, eastern Mediterranean region: subduction, collision, and arc jumping. *Journal of Geophysical Research: Solid Earth, 87*(B9), 7694—7706. https://doi.org/10.1029/JB087iB09p07694.

Salah, M. K. (2017). Lithospheric structure of southeast Anatolia from joint inversion of local and teleseismic data. *Studia Geophysica et Geodaetica, 61*(4), 703—727. doi: 10.1007/s11200-016-1240-7.

Salah, M. K., Şahin, Ş., & Aydin, U. (2011). Seismic velocity and Poisson's ratio tomography of the crust beneath east Anatolia. *Journal of Asian Earth Sciences, 40*(3), 746—761. doi 10.1016/j.jseaes.2010.10.021.

Salah, M. K., Şahin, Ş., & Destici, C. (2007). Seismic velocity and Poisson's ratio tomography of the crust beneath southwest Anatolia: an insight into the occurrence of large earthquakes. *Journal of Seismology, 11*(4), 415—432. doi: 10.1007/s10950-007-9062-2.

Salah, M. K., Şahin, Ş., & Soyuer, D. (2014a). Crustal velocity and Poisson's ratio structures beneath northwest Anatolia imaged by seismic tomography. *European International Journal of Science and Technology, 3*(4), 133—157.

Salah, M. K., Şahin, Ş., &Topatan, U. (2014b). Crustal velocity and V_P/V_S structures beneath central Anatolia from local seismic tomography. *Arabian Journal of Geosciences, 7*(10), 4101—4118. doi: 10.1007/s12517-013-1038-7.

Sandvol, E., Al-Damegh, K., Calvert, A., Seber, D., Barazangi, M., Mohamad, R., Gök, R., Turkelli, N., & Gürbüz, C. (2001). Tomographic imaging of Lg and Sn propagation in the Middle East. *Pure and Applied Geophysics, 158*(7), 1121—1163. https://doi.org/10.1007/PL00001218.

Schmid, C., van der Lee, S., VanDecar, J. C., Engdahl, E. R., & Giardini, D. (2008). Three-dimensional *S* velocity of the mantle in the Africa-Eurasia plate boundary region from phase arrival times and regional waveforms. *Journal of Geophysical Research,* 113, B03306. doi: 10.1029/2005JB004193.

Schmincke, H.-U., Sumita, M., & the Paleovan scientific team. (2014) Impact of volcanism on the evolution of Lake Van (eastern Anatolia) III: Periodic (Nemrut) V_S. episodic (Süphan) explosive eruptions and climate forcing reflected in a tephra gap between ca. 14 ka and ca. 30 ka. *Journal of Volcanology and Geothermal Research, 285*, 195—213. http://dx.doi.org/10.1016/j.jvolgeores.2014.08.015.

Şengör, A. M. C. (1979). Mid-Mesozoic closure of Permo-Triassic Tethys and its implications. *Nature, 279*, 590—593. https://doi.org/10.1038/279590a0.

Şengör, A. M. C., Görür, N., & Saroğlu, F. (1985). Strike-slip faulting and related basin formation in zones of tectonic escape: Turkey as a

case study. In: K. T. Biddle, & N. Christie-Blick (Eds.), *Strike-slip Faulting and Basin Formation* (Vol. 37, pp. 227—264). Soc. Econ. Paleontol. Mineral. Spec. Publ.

Tan, O., Papadimitriou, E. E., Pabuçcu, Z., Karakostas, V., Yörük, A., & Leptokaropoulos, K. (2014). A detailed analysis of microseismicity in Samos and Kusadasi (Eastern Agean Sea) areas. *Acta Geophysica, 62*(6), 1283—1309. doi 10.2478/s11600-013-0194-1.

Tatar, O., Piper, J. D. A., Park, R. G., & Gürsoy, H. (1995). Palaeomagnetic study of block rotations in the Niksar overlap region of the North Anatolian Fault Zone, central Turkey. *Tectonophysics, 244*(4), 251—266. https://doi.org/10.1016/0040-1951(94)00241-Z.

Tatar, O., Piper, J. D. A., Gürsoy, H., Heimann, A., & Koçbulut, F. (2004). Neotectonic deformation in the transition zone between the Dead Sea transform and the East Anatolian Fault Zone, southern Turkey: a paleomagnetic study of the Karasu rift volcanism. *Tectonophysics, 385*(1-4), 17—43. doi: 10.1016/j.tecto.2004.04.005.

Taymaz, T., Yılmaz, Y., & Dilek, Y. (2007). The geodynamics of the Aegean and Anatolia: introduction. In: T. Taymaz, Y. Yılmaz, & Dilek, Y. (Eds.), *The Geodynamics of the Aegean and Anatolia* (Vol. 291, pp. 1—16). Geological Society of London. Special Publication.

Tezel, T., Erduran, M., & Alptekin, Ö. (2007). Crustal shear wave velocity structure of Turkey by surface wave dispersion analysis. *Annals of Geophysics, 50*(2), 177—190.

Tsapanos, T. M., Bayrak, Y., Cinar, H., Koravos, G. Ch., Bayrak, E., Kalogirou, E. E., Tsapanou, A. V., & Vougiouka, G. E. (2014). Analysis of Largest Earthquakes in Turkey and its Vicinity by Application of the Gumbel III Distribution. *Acta Geophysica, 62*(1), 59—82. doi: 10.2478/s11600-013-0155-8.

Warren, L. M., Beck, S. L., Biryol, C. B., Zandt, G., Özacar, A. A., & Yang, Y. (2013). Crustal velocity structure of Central and Eastern Turkey from ambient noise tomography. *Geophysical Journal International*, *194*(3), 1941—1954. doi: 10.1093/gji/ggt210.

Wessel, P., & Smith, W. H. F. (1998). New improved version of Generic Mapping Tools released. *EOS Trans. Am. Geophys. Un., 79*(47), 579—579. https://doi.org/10.1029/98EO00426.

Westaway, R. (1994). Present-day kinematics of the Middle East and Eastern Mediter- ranean. *Journal of Geophysical Research,* 99(B6), 12071—12090. doi: 10.1029/94JB00335.

Yolsal-Çevikbilen, S., & Taymaz, T. (2012). Earthquake source parameters along the Hellenic subduction zone and numerical simulations of historical tsunamis in the Eastern Mediterranean. *Tectonophysics, 536-537*, 61—100. doi: 10.1016/j.tecto.2012.02.019.

Zhao, D. (2001). New advances of seismic tomography and its applications to subduction zones and earthquake fault zones: a review. *Island Arc,* *10*(1), 68—84. https://doi.org/10.1046/j.1440-1738.2001.00291.x.

Zhao, D., Hasegawa, A., & Horiuchi, S. (1992). Tomographic imaging of *P*- and *S*-wave velocity structure beneath northeastern Japan. *Journal of Geophysical Research,* 97(B13), 19909—19928. https://doi.org/10.1029/92JB00603.

Zhao, D., Hasegawa, A., & Kanamori, H. (1994). Deep structure of Japan subduction zone as derived from local, regional and teleseismic events. Journal of Geophysical Research, 99, 22313—22329. https://doi.org/10.1029/94JB01149.

Zhao, D., Tani, H., & Mishra, O. P. (2004). Crustal heterogeneity in the 2000 western Tottori earthquake region: effect of fluids from slab dehydration. Physics of the Earth and Planetary Interiors, 145(1-4), 161—177. https://doi.org/10.1016/j.pepi.2004.03.009.

Zhao, D., Yanada, T., Hasegawa, A., Umino, N., & Wei, W. (2012). Imaging the subducting slabs and mantle upwelling under the Japan Islands. Geophysical Journal International, 190(2), 816—828. https://doi.org/10.1111/j.1365-246X.2012.05550.x.

Zor, E., Sandvol, E., Xie, J., Türkelli, N., Mitchell, B., Gasanov, A. H., & Yetirmishli, G. (2007). Crustal attenuation within the Turkish plateau and surrounding regions. Bulletin of the Seismological Society of America, 97, 151—161. doi: 10.1785/0120050227.